agriculture

MDPI

Article

Design and Experimental Analysis of Straw Suction Unit on Straw Cover Weight Detection Machine

Rongrong Li [1,2], Hongwen Li [1,2,*], Caiyun Lu [1,2], Chao Wang [1,2], Zhengyang Wu [1,3], Zhenwei Tong [1,2], Di Liu [1,3] and Shan Jiang [1,3]

[1] College of Engineering, China Agricultural University, Beijing 100083, China; rrli@cau.edu.cn (R.L.); lucaiyun@cau.edu.cn (C.L.); superc@cau.edu.cn (C.W.); zhengy_wu@cau.edu.cn (Z.W.); tongzhenwei917@163.com (Z.T.); liudi_0929@cau.edu.cn (D.L.); m13324090855@163.com (S.J.)
[2] Scientific Observing and Experiment Station of Arable Land Conservation (North Hebei), Ministry of Agricultural and Rural Affairs, Beijing 100083, China
[3] Key Laboratory of Agricultural Equipment for Conservation Tillage, Ministry of Agricultural and Rural Affairs, Beijing 100091, China
* Correspondence: lhwen@cau.edu.cn; Tel.: +86-10-62737300

Abstract: In response to the issues of high cost, limited detection accuracy, and significant measurement errors inherent in conventional manual techniques used to measure straw cover weight under the conservation tillage method, a dedicated straw cover weight detection machine was developed in the current study. This machine included a critical straw suction device that utilizes negative pressure to collect straw within a defined area. The efficiency of straw collection is affected by suction chamber structural parameters and transport pressure. With crushed corn straw as the research subject, the theoretical calculation of straw suspension velocity was used to determine the wind duct diameter, perform the initial design of the suction chamber structure, and select the appropriate fan. After conducting preliminary experiments, single-factor optimization tests, and orthogonal rotation experiments, we analyzed the flow field distribution patterns and identified the critical parameters for the straw cover weight suction unit. We found that the fan should operate at a speed of 2900 r/min, the diameter of the straw outlet should be 200 mm, the vertical height of the suction chamber should be 536 mm, and the bottom diameter of the suction chamber should be 800 mm. The optimization results were validated through simulation tests and bench tests, yielding an average near-ground airflow velocity of v_j = 9.03 m/s and an average outlet airflow velocity of v_o = 34.27 m/s, meeting the basic requirements of the suction unit. This study could provide a new approach and technical support for the automated detection of straw cover weight in conservation tillage areas.

Keywords: straw cover weight; detection; straw suction unit; CFD simulation; bench test; conservation tillage

Citation: Li, R.; Li, H.; Lu, C.; Wang, C.; Wu, Z.; Tong, Z.; Liu, D.; Jiang, S. Design and Experimental Analysis of Straw Suction Unit on Straw Cover Weight Detection Machine. *Agriculture* **2023**, *13*, 2075. https://doi.org/10.3390/agriculture13112075

Received: 22 September 2023
Revised: 22 October 2023
Accepted: 26 October 2023
Published: 30 October 2023

1. Introduction

Conservation tillage is an advanced agricultural practice that improves soil fertility and helps crops resist drought [1]. It has become the mainstream farming technique in countries such as the United States, Brazil, and China [2]. Among the key technologies of conservation tillage, straw residue cover plays a pivotal role [3]. Residue cover on the soil surface brings several benefits, including reducing water erosion, mitigating wind erosion, increasing soil moisture content, enhancing organic matter content, and reducing dust emissions [4,5]. However, different levels of straw cover over an extended period can impact various soil properties for conservation tillage [6,7], such as soil nutrients and surface moisture content, as well as no-till seeding, crop growth, photosynthesis, yield, soil protection, and weed occurrence. Therefore, the technology for measuring straw cover weight is crucial to ensure compliance with the requirements of conservation tillage.

Currently, there are two main methods for measuring straw cover, namely, straw cover percentage detection and straw cover weight detection [8–18]. Recent research on straw cover percentage detection has involved various image processing and deep learning techniques [19–24]. These methods primarily rely on computer vision to rapidly identify straw-covered areas and process images, which are less labor-intensive and efficient. However, they are susceptible to variations in field conditions, such as differences in straw morphology and lighting, and cannot address the issue of straw uniformity resulting from varying straw cover thickness.

China typically uses manual methods to weigh straw cover, involving collecting samples at specific points using the rope-pulling method. However, this approach is labor-intensive, inefficient, lacks precision in separating straw within and outside the sampling frame, has limited control over detection accuracy, and is prone to measurement error. Currently, there is a lack of research on the mechanization and automation of straw cover weight detection. The author has disclosed a previously published patent titled "A Self-Propelled Straw Cover Weight Detection Machine and Detection Method" [25]. This machine is designed to measure straw cover weight within a fixed area with high precision, replacing manual measurements. The patent provided a detailed description of each working unit, including the straw suction unit.

At present, the main methods of collecting straw in agriculture are mechanical (including two types: spring-tooth drum [26,27] and eccentric telescopic finger-type [28]) and pneumatic [29]. Compared to the mechanical type, the pneumatic type is better suited for uneven terrain, allows for adjustments in wind speed and direction, has higher work efficiency, lower mechanical losses, and reduced maintenance cost. The mechanical type is not very effective at collecting all the straw on the ground because of the large gap between the spring teeth, resulting in a high missed picking rate. Additionally, both mechanical picking types require a lower driving speed, which does not align with the fixed-point picking scheme in this article. Therefore, this paper adopts a pneumatic straw suction method. The suction chamber and air duct transport system's inner diameter, fan selection, and suction chamber design are crucial for the straw collection rate. Pneumatic conveying systems have been widely applied in agricultural production in recent years, with research focusing on the pneumatic conveying characteristics of various agricultural biomaterials [30], including pipeline design and analysis of different biomass particles and the study of complex situations involving the movement of biomass particles in multiphase flow [31–34].

In this paper, we discuss a study on the suction chamber model using CFD software (version 2024). This research includes simulation tests that illustrate the movement of straw within the airflow field present inside the suction chamber. The test results and simulation analysis offer valuable insights for designers and engineers to optimize the suction chamber structure. CFD can simulate, calculate, and analyze flow fields [35]. CFD has been utilized in various agricultural applications, such as predicting fluid flow and heat transfer during grain drying to improve product quality [36]. CFD has also been used to simulate and evaluate complex environmental parameters within intensive agricultural production systems [37].

In this paper, the straw cover weight detection machine employs the straw cover weight unit, which operates using a dilute-phase pneumatic conveying method. (When the concentration of particles in the airflow is below 0.05 m^3/m^3, the solid-to-gas ratio is low, resulting in high power consumption and fast material flow rate) [38]. The high-speed rotation of the centrifugal fan induces air to move centrifugally, creating a pressure differential within the air due to centrifugal force. This results in the formation of negative pressure inside the suction chamber. As the airspeed within the suction chamber reaches the suspension velocity (When fluid blows particles from the bottom to the top at a specific speed, the particles will remain stationary. The speed at which the fluid blows upward in order to achieve this is known as the suspension speed of the fluid. If the fluid speed is greater than the suspension speed, the particles will be carried away.) of the straw cover

weight on the ground [39], it transports the straw cover weight from the suction chamber into the fan and through the ducts, ultimately reaching the collection bag.

Following an analysis of the factors influencing the efficiency of straw cover weight suction, the determination of duct diameter, initial design of the suction chamber, and fan selection were all based on the straw cover weight suspension velocity. Furthermore, a CFD model was established, enabling numerical simulations and an examination of airflow patterns within the suction chamber. This investigation led to the identification of optimal operating conditions and crucial parameters for the suction chamber structure. These findings provide a foundation and reference for the design and optimization of the straw cover weight suction unit within the straw cover weight detection machine.

2. Materials and Methods

2.1. Structure and Working Principle of the Straw Cover Weight Detection Machine's Straw Suction Unit

The straw cover weight detection machine mainly includes the following components: the mobility unit, straw cutting unit, straw suction unit, straw cleaning unit, weighing unit, and control unit, as shown in Figure 1. The control unit coordinates multiple units of the detection machine for real-time measurement of straw coverage in multiple areas. The mobility unit, using a satellite positioning system, scans the field map of the target area and transfers it to a mobile app. The machine's built-in program then plans the optimal path to reach each specified measurement area, as illustrated in the process flow of the mobility unit in Figure 2. The straw cutting unit separates the straw inside and outside the sampling frame using cutting blades, with adjustable frame height. The straw suction unit utilizes a negative pressure pneumatic conveying system, along with air ducts and an axial-free screw conveyor, to transport the straw within the sampling frame to the double-layer straw sieving cylinder of the straw cleaning unit for the removal of impurities. The effectiveness of the air duct transportation system, especially in terms of cleaning surface straw within the target area, determines the quantity of straw transported to the straw cleaning unit. This quantity, in turn, determines the straw weight measured by the weighing unit. Therefore, the straw suction unit is a crucial component for ensuring accurate measurement results and represents the core focus of this study.

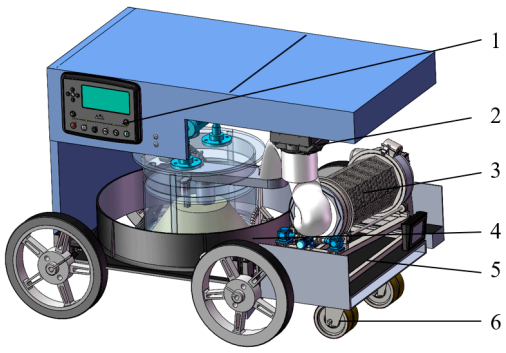

Figure 1. Three-dimensional model diagram of straw cover weight detection machine. 1. Control unit; 2. Straw suction unit; 3. Straw cleaning unit; 4. Straw cutting unit; 5. Weighing unit; 6. Walking unit.

Figure 3 illustrates the framework of the straw suction unit, which includes a suction chamber, inverter, intake air duct, centrifugal fan, exhaust air duct, chassis, frame, and collection bag. The centrifugal fan comprises the motor, snail shell, impeller, and blades. In case of any issue, one can replace individual suction chamber units by disconnecting the connection between the stalk outlet and the air inlet duct, and then replacing it. The diameter of the intake air duct and the intake opening of the centrifugal fan must match the diameter of the suction chamber's straw outlet. The first two components can also be replaced, and the structural parameters can be adjusted by conducting multiple bench tests.

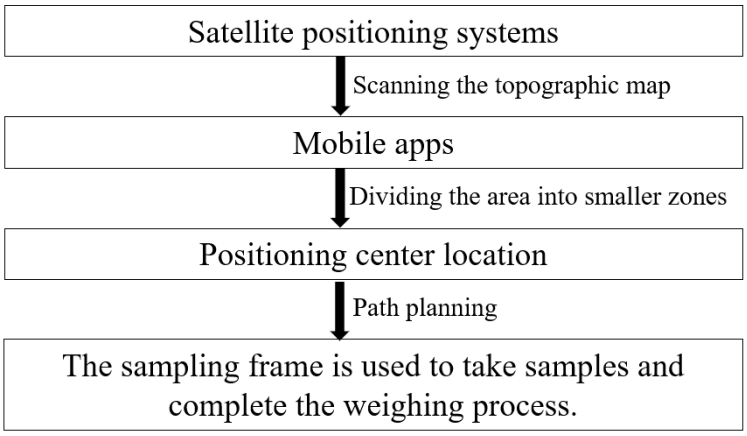

Figure 2. Flowchart illustrating the execution process of the walk unit.

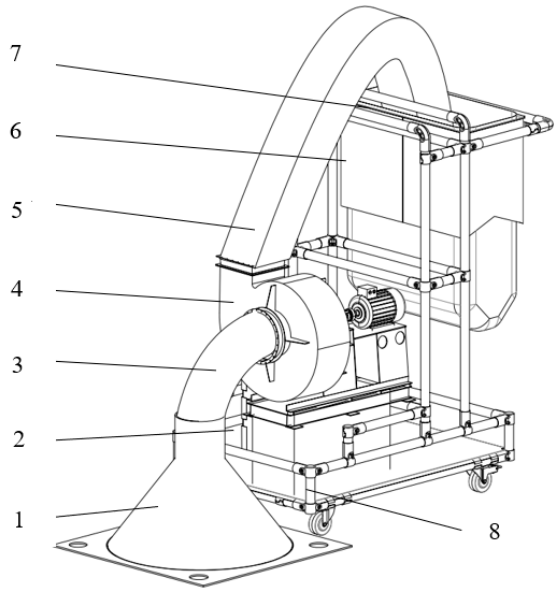

Figure 3. Straw suction unit bench structure. 1. Suction cavity; 2. Inverter; 3. Air intake duct; 4. Centrifugal fan; 5. Air outlet duct; 6. Collection bag; 7. Frame; 8. Chassis.

During operation, straw is conveyed from the ground surface into the collection bag through the interior of the suction chamber, intake air duct, fan, and exhaust air duct. The suction chamber is positioned 10 mm above the ground, and its bottom area corresponds to the measurement area of the detection machine. The inverter controls the centrifugal fan's speed, gradually increasing it. When the centrifugal fan starts, a pressure difference is formed between the inside and outside of the suction chamber. Once the airflow velocity inside the suction chamber reaches the starting speed of the straw, the straw starts to move. Due to the gradually tapered structure of the suction chamber, the straw in the central area of the ground reaches the starting speed first, while the straw in the edge area near the bottom of the suction chamber follows suit. With the increase in the centrifugal fan's speed and airflow volume, the pressure difference between the inside and outside of the suction chamber increases. When the airflow velocity inside the suction chamber exceeds the suspension velocity of the straw, a high-speed negative pressure airflow lifts the ground straw upward. The straw adopts a rotating upward posture within the suction chamber, and some straw may impact the interior wall of the suction chamber. Ultimately, the straw reaches the suction chamber's straw outlet at the bottom. After entering the centrifugal fan through the intake air duct, the straw, under the rotation of the impeller

blades and the influence of the airflow, arrives at the exhaust air duct and finally reaches the collection bag.

2.2. Straw Sucking Process Theoretical Analysis

During pneumatic conveying, the movement of materials can be quite complex. The straw located at the circular bottom of the suction chamber experiences various situations, including friction with the pipe wall during upward movement. This can lead to scenarios such as dense flow, sparse flow, and stagnant flow. However, the straw located near the center of the projection circle at the bottom of the suction cavity is considered to be in the vertical suction cavity. Once the straw is sucked up, the distribution in the suction cavity tends to be uniform [40]. In order to study the factors that affect the effectiveness of straw suction, an analysis was conducted on the forces that act on the straw in the direction of flow along the suction chamber wall.

As shown in Figure 4, within the inclined suction chamber wall with a slope angle θ, there is a group of particles distributed along the ΔL segment, represented by n particles. Assuming that each of the n particles experiences a force equivalent to the force on a single particle, the particle group is subjected to the thrust force nf from the airflow and its own weight nw. The gravitational force component acting in the direction of the flow is $nw\sin\theta$. Due to the complex nature of wall forces, it is assumed that the frictional force is proportional to the force in the vertical direction of the wall due to gravity. Let the friction coefficient be ξ. Therefore, the frictional force in the direction of flow is $\xi nw\cos\theta$. When the particles reach their suspension velocity, the degree of friction between the particles and the wall decreases, and a layer of air cushion is formed between the particle group and the wall. At this point, the approximate reaction force from the wall is the gravitational force component $nw\cos\theta$. For a particle group with an airflow velocity of v_a and an initial velocity of 0, being accelerated to a certain velocity $v_{b,}$ the equation of motion for the particle group is as follows:

$$n\frac{w}{g}\frac{dv_b}{dt} = nw - \xi nw\cos\theta - nw\sin\theta \tag{1}$$

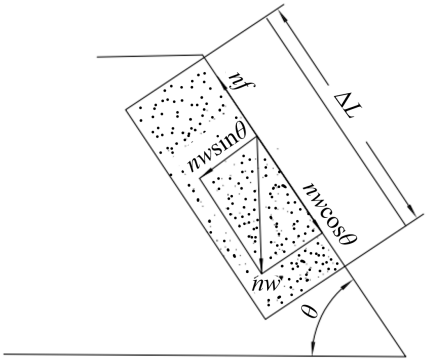

Figure 4. Schematic diagram of straw forces.

By using the velocity ratio $\phi = \frac{v_b}{v_a}$, Equation (1) can be rearranged as follows:

$$\frac{d\phi}{dt} = g\frac{v_a}{(v_a - v_b)^2}\left[\phi^2 - 2\phi + \{1 - \left(\frac{v_a - v_b}{v_a}\right)^2(\xi\cos\theta + \sin\theta)\}\right] \tag{2}$$

When the particles are accelerated to a certain velocity and reach a stable conveying state, $\frac{d\phi}{dt} = 0$, that is, when:

$$\phi = 1 - \left(\frac{v_a - v_b}{v_a}\right)(\xi\cos\theta + \sin\theta)^{\frac{1}{2}} \tag{3}$$

To achieve good straw suction performance and high suction efficiency while ensuring that the straw can be lifted, it is essential for the straw to reach a stable conveying state within a relatively short period. In other words, the time it takes for the velocity ratio ϕ to approach 1 should be minimized. As indicated by Equation (3), the increase in velocity ratio ϕ during the straw suction process is related to the air velocity v_a and the inclination angle θ of the suction chamber, assuming that v_b and ξ are constant values [41]. As shown in Figure 5, the inclination angle θ is determined by three structural parameters of the suction chamber: the vertical height H, the outlet diameter D, and the bottom diameter L. According to experimental data from researchers like Prandtl [42], Nikuradse [43], and Reichardt [44], it has been observed that at different distances from the pipe wall, materials experience varying degrees of air thrust and friction velocity, leading to different motion states. This study describes a tapered suction cavity. As the height of the cavity increases, the cross-sectional area decreases. Consequently, the airflow velocity and acceleration values increase continuously. This design can also impact the air velocity v_a and, consequently, it can influence the straw suction performance.

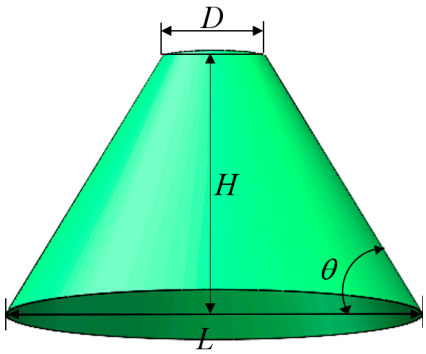

Figure 5. A schematic diagram of the suction chamber structure.

In addition, the collision between particles or between particles and the pipe wall results in the loss of some kinetic energy gained from the airflow thrust. This is manifested as pressure loss, which affects the airflow velocity v_a. Therefore, in the following sections, pressure loss will be calculated as a basis for selecting an appropriate fan and studying the impact of the fan's suction (negative pressure) on the airflow velocity.

2.3. Key Component Design

There are two main types of pneumatic conveying methods—suction-type and pressure-type [41]. These methods are further divided into dense-phase conveying and dilute-phase conveying based on material density. The first step in designing a pneumatic conveying system is to accurately calculate the pressure loss within the transportation system. This calculation is crucial in designing various components of the apparatus and can have a significant impact on the overall quality and equipment costs. In this study, considering the density of straw and the design concept, the suction-type dilute-phase pneumatic conveying method has been adopted.

Surface straw primarily consists of leaves and stems, with stem suspension velocity greater than leaf suspension velocity [45]. Therefore, in the subsequent calculation process aimed at meeting the conditions for transporting straw and improving the efficiency of straw transport, the suspension velocity of straw stems can be used as a reference. Based on the straw suspension velocity, calculations for duct diameter, preliminary design of the suction chamber structure, pressure loss within the transport pipes, and fan selection were conducted.

2.3.1. Straw Suspension Velocity

Considering the fluid dynamics' characteristics of irregular materials, a force analysis was performed when straw was suspended. It was subject to forces such as its own gravity,

drag force from the airflow, and buoyancy. Using the method recommended by ASAE, irregularly shaped materials are simplified to equivalent spheres with unchanged volume and density [46].

When the material reached the critical velocity, it was in equilibrium under the influence of these three forces, and they were equal to each other:

$$C_s A_s \rho_f {v_{ts}}^2 = mg - \frac{m}{\rho_s}\rho_f g \tag{4}$$

The equations for the equivalent sphere diameter d_e, shape correction factor Φ, and suspension velocity of the equivalent sphere v_{te} were as follows:

$$\begin{cases} d_e = 1.24\left(\frac{m}{\rho_s}\right)^{1/3} = 1.24 v_p^{1/3} \\ v_{te} = \sqrt{\frac{4gd_e(\rho_s-\rho_f)}{3C_e\rho_f}} \\ v_{ts} = \frac{1}{\sqrt{\phi}} v_{te} = \frac{1}{\sqrt{\phi}}\sqrt{\frac{4gd_e(\rho_s-\rho_f)}{3C_e\rho_f}} \end{cases} \tag{5}$$

where m is the mass of straw (kg); g is the acceleration due to gravity (m/s^2); ρ_s is the density of straw (taken as 100 kg/m^3); v_p is the volume of straw (m^3); ρ is the density of air (1.25 kg/m^3); A_s is the windward area of straw (the projected area in the vertical direction of material movement) (m^2); v_{te} is the suspension velocity of the equivalent sphere (m/s); C_S is the straw drag coefficient; C_e is the equivalent sphere drag coefficient; v_{ts} is the suspension velocity of straw (m/s); and Φ is the shape correction factor (taken as 0.75) [47].

From Equation (5), it can be observed that when the fluid density (ρ), straw density (ρ_s), and shape correction factor (Φ) are determined, the suspension velocity (v_{ts}) is only related to the equivalent diameter (d_e) and the equivalent sphere drag coefficient (C_e). The equivalent sphere diameter (d_e) is determined by the straw volume (v_p).

A five-point sampling method was used to determine five sampling areas of 1 m^2 each. The experimental samples were corn straw collected in November 2022 after the straw return operation in the test field in Harbin, as shown in Figure 6. Random samples of equal weight were taken from each of the five sampling areas, and their moisture content was measured using a drying method, resulting in values of 7.783%, 8.973%, 7.063%, 6.966%, and 6.880%. The average moisture content was 7.533%. To facilitate theoretical calculations, the corn stalk portion was simplified to a cylinder. From each sampling area, 40 random stalks were selected, totaling 200 stalks as calculation samples. The diameter d and length l of each stalk were measured, and their volumes were calculated. Stalks from different parts of the straw have varying cross-sectional areas, leading to different v_p values. Based on the measurement results, it was determined that 95% of the crushed corn stalks had diameters between 4 mm and 18 mm, and 90% of them had lengths between 60 mm and 100 mm. The average sample volume was calculated as $v_p = 6.34 \times 10^{-6}$ m^3 and $d_e = 0.022$ m.

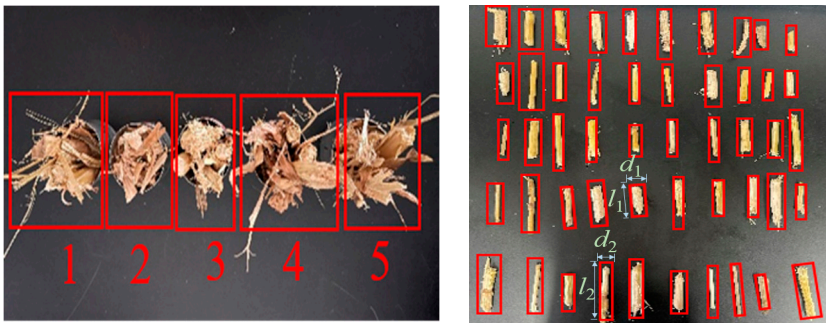

(**a**) (**b**)

Figure 6. Test sample. (**a**) Straw sample; (**b**) Straw stalk sample.

The drag coefficient C_e is related to the Reynolds number R_e. Referring to agricultural material parameters and calculating with the Reynolds number [48], it is determined that $R_e > 500$. In the Newtonian drag region where $500 < R_e < 2 \times 10^5$, the drag coefficient is relatively constant, approximately 0.44. When $R_e > 2 \times 10^5$, it reaches the critical drag region, and the drag coefficient suddenly decreases by approximately 50%. The drag coefficient follows the formula $C_e = 1.194 - 0.13\varepsilon$, where ε represents the angle between the stalk's normal direction and the relative velocity direction, ranging from 0° to 90°. From Equation (5), it can be observed that C_e is inversely proportional to ε. Therefore, when $\varepsilon = 0°$, which means that the stalk's normal direction is aligned with the airflow direction, the drag coefficient is a maximum, denoted as $C_{emax} = 1.194$. When $\varepsilon = 90°$, meaning that the stalk's normal direction is perpendicular to the airflow direction, the drag coefficient is a minimum, denoted as $C_{emin} = 0.024$.

Substituting these values into Equation (5), it is calculated that 5.081 m/s < v_{ts} < 11.813 m/s.

2.3.2. Duct Diameter Design

The duct diameter d is determined by the conveying air velocity v_a and the required air volume for conveying Q_a, expressed by the formula:

$$d = \sqrt{\frac{4Q_a}{\pi v_a}} \tag{6}$$

where v_a is based on the relationship table between conveying air velocity v_a and critical velocity v_{ts} of materials [49]. In order to ensure the intake rate of surface straw, $v_a = 1.9v_{ts}$ is selected; thus, 9.654 m/s < v_a < 22.479 m/s.

The required air volume for conveying, Q_a, is calculated as W_a/ρ_f, where W_s represents the air mass required for conveying in a unit of time. It is determined by the mixture concentration ratio u_s and the mass of material W_s transported in unit time. u_s is calculated as W_s/W_a. In order to enhance the conveying capacity, the total amount of surface straw transported by the air duct transportation system is designed to be a maximum of 1 m^2, with a total weight of approximately 1.3 kg. Therefore, the maximum W_s should be 1.3 kg/s. Considering that the actual transported straw material can be approximated as cylindrical and the conveying conditions are low-vacuum attracting, a mixture ratio u_s of 1.6 is selected based on reference to other relevant examples. Thus, W_a is 0.81 kg/s.

2.3.3. Suction Chamber Preliminary Design

Suction-type conveying systems commonly use suction nozzles, including single-tube nozzles, double-tube nozzles, and rotating nozzles. Single-tube nozzles include straight tube nozzles, bell-mouth nozzles, and oblique-mouth nozzles. To reduce energy loss, a single-tube bell-mouth nozzle with a simple structure, low mixing ratio, and minimal resistance loss is selected. This type of nozzle is a gradually tapered conical suction chamber.

In order to save power, facilitate subsequent processing of the suction chamber, and make the bottom area closer to an integer value for ease of calculation, the suction chamber's bottom area was set at 0.5 m^2, and the bottom diameter L was designed to be 800 mm. Since the suction chamber is connected to the air duct at the straw outlet, the diameter D of the straw outlet is determined based on the calculated results of the air duct's inner diameter. The suction chamber's height H is determined based on the height of the chassis of the straw cover weight detection machine and the selected fan's outlet center height. The slope θ ranges from 0° to 90°. When calculating pressure loss, the maximum values of the suction chamber's structure were used to meet the requirements for subsequent straw suction.

In the following text, the suction chamber structural parameters are optimized through preliminary experiments and CFD simulations.

2.3.4. The Choice of Fan

During the conveying process, various practical factors can lead to a decrease in pressure, which is referred to as pressure loss. This pressure loss primarily occurs in two parts during the suction of straw: within the suction cavity and along the intake air duct. The design involves a circular duct from the suction cavity outlet to the fan inlet. The total pressure Δp includes both static pressure Δp_s and dynamic pressure Δp_t, expressed as $\Delta p = \Delta p_s + \Delta p_t$, where dynamic pressure represents the pressure due to kinetic energy and can be defined as $\Delta p_t = 0.5\rho_f {v_a}^2$. Static pressure encompasses several types of pressure losses, including acceleration pressure loss Δp_j, frictional pressure loss Δp_q, local pressure loss Δp_b, and suspension pressure loss Δp_m [50]. Specifically, acceleration pressure loss mainly occurs during the acceleration of straw within the suction cavity [51]. Frictional pressure loss results from the friction between the fluid and the cavity walls and occurs within the suction cavity and material conveying ducts. It is the difference in pressure between the inlet and outlet. Local pressure loss is primarily caused by changes in cross-sectional shapes within the duct and variations in inlet and outlet sections. Suspension pressure loss is mainly related to the lifting and suspension of materials and is governed by the following Formulas (7):

$$\begin{cases} \Delta p_j = (1 + \frac{\rho_f v_a^2}{2} + \int_{0.2}^{1} \frac{2W_s v_{ts}}{\pi d^2} \mathrm{d}d + 3C \frac{{\rho_f}^2}{\rho_s - \rho_f} \frac{u_s v_{ts}}{2d_e} (1 - \frac{4\rho_f u_s}{\rho_s - \rho_f})^{-4.7} \\ \Delta p_q = p_1 - p_2 \\ \Delta p_b = \Delta p_{b1} + \Delta p_{b2} \\ \Delta p_m = u_s \rho_s l \frac{v_f + v_s \sin\theta}{v_s} \end{cases} \quad (7)$$

where C is the air dynamic resistance coefficient of straw, with a maximum value of 1.194 as determined earlier; l is the length of the intake air duct, measured in meters (m); v_s is the velocity of material particles, measured in meters per second (m/s); v_f is the suspension velocity within the intake air duct, measured in meters per second (m/s); and θ is the pipe inclination angle, which is substituted here with the $\sin\theta$ maximum value of 1.

After calculations, the Δp_t is 330.63 Pa, the Δp_j is 406.94 Pa, the Δp_q is 109.77 Pa, the Δp_b is 119.03 Pa, the Δp_m is 168.81 Pa, and the theoretical total pressure loss is 1134.858 Pa. Considering other losses along the path and ensuring a 40% increase in the total pressure to account for straw cleaning, the corrected total pressure is 1907.11 Pa. To select an appropriate fan, you need to calculate the fan's airflow rate (Q, in m^3/h), air pressure (P, in Pa), and power (W, in kW) using the following expressions:

$$\begin{cases} Q = \varphi Q_a \\ P = \varphi \Delta p \\ W = \frac{QP}{3600 \times 1000 \times \eta_1 \eta_2} \end{cases} \quad (8)$$

where Q is the theoretical required air volume (m^3/h); ϕ is the design margin, taken as 1.2; η_1 is the fan efficiency, taken as 0.75~0.85; and η_2 is the mechanical transmission efficiency, taken as 1.

2.4. Suction CFD Simulation Experiments

Based on the calculations and design results for the components of the straw cover weight suction unit in Section 2.3, the following values were determined: the suction chamber ground diameter L is 800 mm, the suction chamber height H is most suitable in the range of 400 mm to 700 mm, and the outlet diameter D should fall between 190 mm and 200 mm. For H, based on a significant number of preliminary experimental results, narrowing it down to the range of 450 mm to 650 mm resulted in better straw cover weight suction performance. To further investigate the optimal operating conditions and key

combination parameters for the suction chamber structure, a CFD model was established for the suction chamber and CFD simulations were conducted.

2.4.1. CFD Model Construction

Using CFD simulations to determine the optimal suction chamber structural parameters, a suction chamber model was established in a 1:1 scale using SolidWorks three-dimensional design software (version 2023).

Because parameters at the inlet around the bottom of the suction chamber were unknown, and the airflow patterns were complex, an extended area was established. The height of the extension area had minimal impact on the results and was set to 50 mm, which was the same as the gap between the suction chamber and the ground. The radius was set to three times the suction inlet radius, which was 1200 mm. The mesh was generated using the meshing method provided by Workbench 2020 R2, utilizing unstructured meshing. Mesh quality was assessed using the skewness mesh metric, with a maximum value set at 0.85. The results indicate that the mesh quality was good, with more than 2 million mesh elements, as shown in Figure 7. Since the fan pressure affects the suction force, and thus the straw suction efficiency and airflow velocity distribution within the suction chamber, and considering that the fan pressure can be adjusted, the simulated outlet pressure parameters were set to −2500 Pa to −3500 Pa, based on the minimum calculated fan pressure when the outlet diameter was 200 mm, which was 2312.5 Pa. Because the pressure difference inside the suction chamber generates airflow for straw suction, the boundary condition for the chamber's bottom was set as pressure inlet (0 Pa), and the straw outlet was set as pressure outlet with actual negative pressure values.

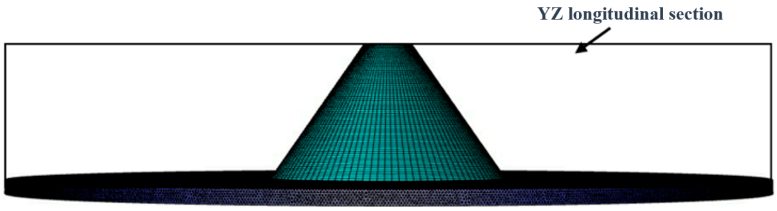

Figure 7. Suction chamber and extended area mesh diagram.

In the Fluent simulation process, a three-dimensional turbulent numerical simulation method, specifically the Reynolds-Averaged Navier–Stokes (RANS) method, was employed. The core of the RANS method involves solving the time-averaged Reynolds equations, which is currently one of the most widely used turbulent numerical simulation methods. In this simulation experiment, the Realizable k-ε turbulence model was utilized. This model was suitable for this study because it relates the strain rate to the turbulent viscosity calculation and accommodates the varying cross-sections in the suction chamber. The numerical computation of the flow field was carried out using the SIMPLE (Semi-Implicit Method for Pressure-Linked Equations) algorithm. This algorithm was based on solving the discretized form of the momentum equation with a given pressure field. It iteratively corrects the pressure values to obtain a new velocity field until the velocity field converges. The SIMPLE algorithm is known for its strong stability, robustness, and wide applicability. Solver method: simple, with strong stability, robustness, and wide applicability. The control equations were discretized using the Green–Gauss cell-based method with a second-order upwind scheme. The simulation was run for a total of 2000 iterations (Table 1).

2.4.2. Evaluation Criteria

Once the bottom diameter L is determined, the slope θ is solely determined by the exit stem diameter D and the height H. Therefore, it is considered that the optimal slope θ_s formed by the height H_s and exit stem diameter D_s in the best simulation results is the optimal solution. Generally, as the conveying air velocity increases, the material distribution

inside the conveying pipe becomes more uniform; when the air velocity decreases, the material tends to be more densely packed near the bottom.

Table 1. CFD Simulation Gas Phase Parameters.

Parameters	Value
Medium	air
Acceleration of gravity/(m/s^2)	9.81
Density/(kg/m^3)	1.25
Temperature/(°C)	25
Viscosity/(kg/(m/s))	1.7984×10^{-5}
Time step/(s)	2×10^{-3}

To avoid the occurrence of material clumping at the bottom of the suction chamber due to low air velocity, indices such as the average near-ground air velocity v_j, exit air velocity v_o, and the average air velocity v_m in the YZ longitudinal section of the suction chamber are used to assess the ability of airflow to transport straw. A larger v_j, v_o, and v_m indicate better straw transport. Preliminary experimental results show that the maximum flow cross-section in the entire suction chamber is in the vertical YZ section in the middle of the chamber. The uniformity index of the velocity in the YZ longitudinal section, denoted as γ_v [52], is used to evaluate the overall velocity uniformity within the suction chamber. A larger γ_v indicates more uniform air velocity distribution within the suction chamber, and it is expressed as follows:

$$\gamma_v = 1 - \frac{1}{2n} \sum_{j=1}^{n} \frac{\sqrt{(v_j - \overline{v})^2}}{\overline{v}} \tag{9}$$

2.4.3. Design of Single-Factor Optimization Experiments

To narrow down the optimal range of suction chamber vertical height (H) and understand its impact on airflow velocity, the range of H obtained from preliminary experiments was divided into five horizontal gradients: 450 mm, 500 mm, 550 mm, 600 mm, and 650 mm. Single-factor experiments were conducted with the straw outlet diameter set at 200 mm, the bottom diameter set at 800 mm, and the negative pressure at the straw outlet set at −2500 Pa. Simultaneously, the corresponding angles (θ) of the suction chamber were set to 56.31°, 59.09°, 61.35°, 63.43°, and 65.26°, respectively. The experimental results were analyzed to determine the optimal range for the vertical height (H) value.

2.4.4. Design of Orthogonal Rotational Combination Experiments

As indicated in Section 2.2, the factors affecting airflow velocity are the suction chamber structure and transport pressure. Once the bottom diameter of the suction chamber is determined, the parameters that determine the suction chamber structure are the vertical height (H) and the straw outlet diameter (D) of the suction chamber. The transport pressure, represented by the pressure at the straw outlet (P), has a significant impact on straw transportation in the simulations. Therefore, three parameters, D, H, and P, were chosen as experimental variables. The factors were studied with three levels each, resulting in a total of 15 experimental combinations, using v_j, v_o, v_m, and γ_v as indicators. The levels of the experimental factors are presented in Table 2. Among them, H was determined to have a range of 500 to 650 mm based on single-factor experiments. The straw outlet diameter (D) had a test range of 190 to 200 mm, considering the duct diameter and the selected fan. The transport pressure (P), determined by the fan's wind pressure, had a test range of −2500 to −3500 Pa. The experimental results were analyzed, and the optimization outcomes were validated through simulation experiments and bench tests.

Table 2. Orthogonal experimental factor level table.

Level	Factors		
	Straw Outlet Diameter *D*/mm	**Vertical Height *H*/mm**	**Transport Pressure *P*/Pa**
1	190	500	−2500
2	195	550	−3000
3	200	600	−3500

2.5. Design of the Straw Suction Unit Bench Test

To test the reliability and operational effectiveness of the straw suction unit, bench validation tests were conducted in the indoor laboratory of the Conservation Tillage Research Center at China Agricultural University.

The whole test bench, as depicted in Figure 8, consisted of a small car chassis (1300 mm × 1000 mm), polyurethane air ducts, a centrifugal fan from the 06-46 3.6A type, a collection pipe, and the suction chamber. A uniform sample of 1.3 kg of straw was spread on the ground with a diameter of 800 mm, and the suction chamber was placed 1 cm above the corresponding straw location. To measure the airflow velocity, air volume, and pressure within the suction chamber, the following steps were followed. First, the researchers waited until the fan speed stabilized. The wind speed, air volume, and pressure tester were then placed parallel to the ground at the bottom of the suction chamber. The measuring end of the tester was inserted 100 mm, 200 mm, and 300 mm from the edge of the suction chamber. Six testers were selected evenly spaced along the circumference and measured at 400 mm from the edge of the suction chamber, which was the center of the bottom of the suction chamber. Each measurement lasted approximately 15 s, or until the tester showed a stable number. The data for each point were recorded. There were 19 wind speed values per group of tests. To obtain the average velocity v_j of airflow near the ground, the average value for each group of wind speed was calculated. To measure the average air flow speed v_o at the stalk outlet, the wind speed, air volume, and pressure tester were inserted into the air duct at the outlet of the suction cavity. The measurement was made the same way as for the average air flow speed near the ground.

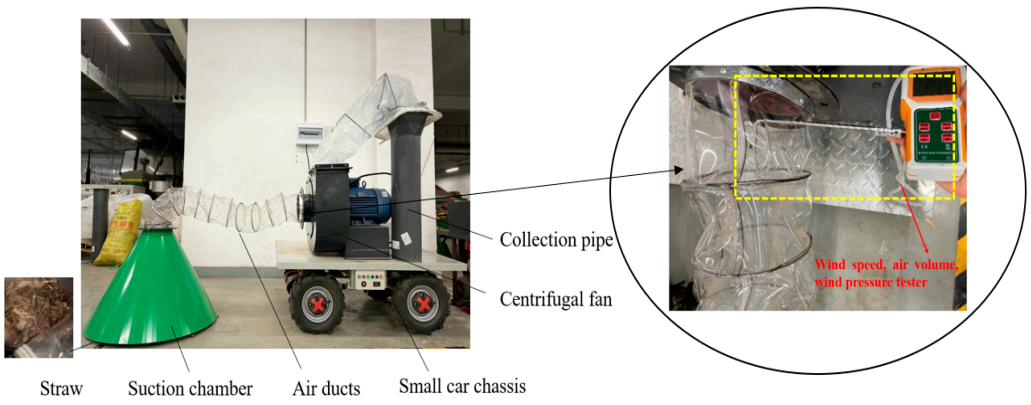

Figure 8. The setup of the bench test for the straw suction unit.

3. Results and Discussion

3.1. Determining the Diameter of the Air Duct and Selecting the Fan

Based on the parameters from Section 2.3.2, a calculation yielded the required air volume for conveying Q_a as 0.65 m^3/s, and d was 0.19 m. For the convenience of calculation in the subsequent text, d was approximated as 0.2 m.

Based on the parameters from Section 2.3.3, Q was 2808 m^3/h, P was −2288.53 Pa, and W was 2.23 kW. For the fan selection, a type 06-46 3.6A centrifugal fan was chosen

for the experiment. The specific parameters of this fan were as follows: air volume of 3000 m^3/h, air pressure of 3500 Pa, electric motor power of 5.5 kW, left rotation by 90°, main shaft speed of 2900 r/min, and the speed could be adjusted through an inverter to control the air pressure effectively. This choice was made to meet the performance requirements for straw suction, accommodate varying moisture levels in straw across different areas, and allow for a wide range of air volume adjustments during the experiment.

3.2. Results and Analysis of Single-Factor Experiments

Figures 9–12 display the results of the simulation.

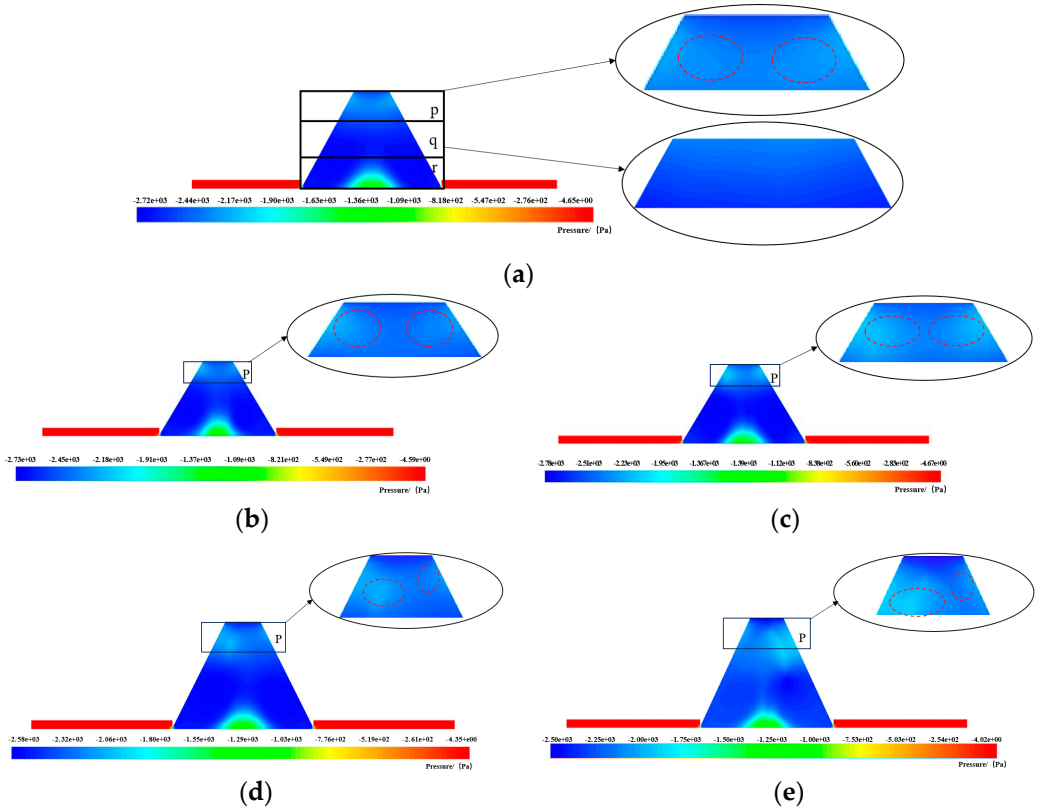

Figure 9. Static pressure contour map of suction chamber YZ cross-section. (**a**) H = 550 mm; (**b**) H = 450 mm; (**c**) H = 500 mm; (**d**) H = 600 mm; (**e**) H = 650 mm.

According to Figure 9, based on the overall distribution of negative pressure, the YZ cross-section of the suction chamber is divided into three regions, labeled p, q, and r, representing the upper, middle, and lower parts of the suction chamber, respectively. In the bottom part of the suction chamber (region r), where the expansion area was connected to the external atmosphere, the static pressure remained minimal and close to 0, as depicted in Figure 10, where the airflow velocity in the expansion area was also 0. As the airflow entered the connection point between the expansion area and the suction chamber, there was a sudden increase in negative pressure, leading to a rapid increase in airflow velocity, as shown in Figure 12, with the airflow velocity reaching its peak at the outermost periphery near the suction chamber entrance. As the airflow converged toward the center from the surrounding areas, collisions between airflow particles occurred, resulting in energy loss. This led to a decrease in negative pressure of approximately −1360 Pa in the central area near the ground, indicated by the green region in Figure 9. In this central region, the airflow experienced the greatest energy consumption, resulting in the lowest airflow velocity near the ground. In the middle region (region q) of the suction chamber, the negative pressure gradually decreased as it transitioned to the upper part of the suction chamber (region p). The negative pressure decreased from around −2500 Pa to approximately −2200 Pa, and this reduction became more pronounced as the suction chamber height increased. In the

upper part of the suction chamber (region p), the negative pressure gradually decreased, forming a gradient, as observed in Figure 9. However, near the suction chamber's exit where the negative pressure suddenly increased, there was a decrease in negative pressure as the airflow accelerated and converged toward the exit. This phenomenon was accompanied by an increase in airflow velocity. Near the exit, the airflow converged and resulted in higher airflow velocity values, as shown in Figure 11e,f.

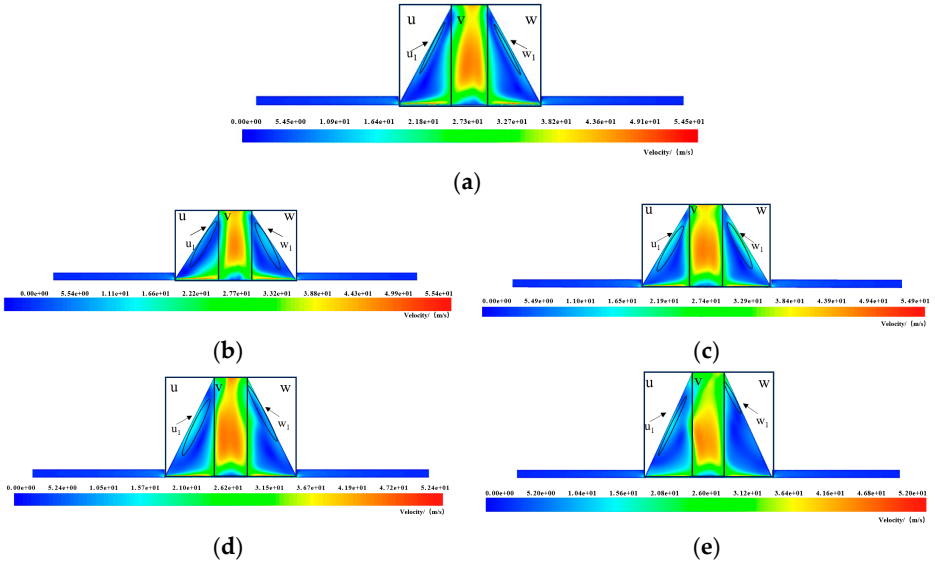

Figure 10. Velocity contour map of suction chamber YZ cross-section. (**a**) H = 550 mm; (**b**) H = 450 mm; (**c**) H = 500 mm; (**d**) H = 600 mm; (**e**) H = 650 mm.

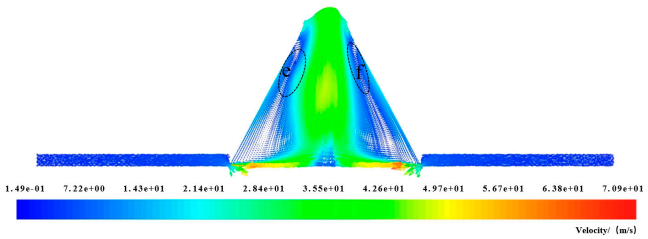

Figure 11. Velocity vector map of suction chamber YZ cross-section.

Figure 10 reveals that the airflow velocity in the vertical region of the suction chamber (v) has higher values compared to the side regions (u, w), forming a distinct boundary. A prominent feature was the red-colored high-speed airflow column, which can be approximated as a vertical suction chamber with airflow velocities exceeding 50 m/s. This high airflow velocity suggests that the straw should be transported relatively uniformly in this section. The reason for this phenomenon was that the airflow gathered toward the exit as it moved upward. In contrast, the airflow velocities in regions u and w were lower due to collisions with the suction chamber walls. Some of the airflow in the u_1 and w_1 regions collided with the chamber walls and then recirculated, resulting in a relatively smaller decrease in airflow velocity. As shown in Figure 12, the airflow velocity near the ground in the central area was the lowest, with values ranging from 7 m/s to 10 m/s, slightly below the suspension velocity of the straw. This indicates that it may not be favorable for the intake of straw in the central position of the test area. However, excluding the central area, the peripheral areas of the suction chamber expansion met the requirement of having airflow velocities greater than the suspension velocity of the straw, ensuring that the majority of the straw was drawn in.

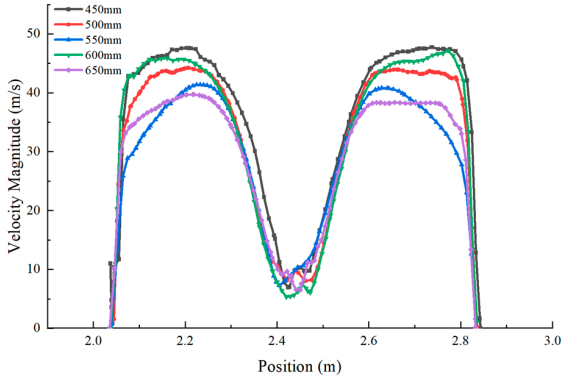

Figure 12. Velocity profile of near-ground airflow at the suction chamber inlet.

Table 3 summarizes the data and Figure 13 shows the results of various height indicators. It can be observed that as the height (H) increases, the slope (θ) also increases, with an increase of approximately 2° for every 50 mm increase in height. The values of v_j, v_o, v_m, and γ_v initially increased and then decreased as H increased. The percentage increases for v_j, v_o, v_m, and γ_v were 7.79%, 6.25%, −3.27%, −4.25%, 0.98%, 0.5%, −2.43%, −3.52%, 8.63%, −3.97%, −1.37%, and −4.49%, respectively. Overall, the change in slope resulted in minimal fluctuations in v_o and v_m, and moderate fluctuations in v_j and γ_v. Among these indicators, v_j, v_o, and γ_v reached their peaks at H = 550 mm, while v_m peaked at H = 500 mm. This indicates that excessively large or small slopes results in poor straw transport efficiency. A lower height (H) and smaller slope (θ) caused the airflow to rise more slowly along the chamber wall, leading to more collisions with the wall and a higher collision frequency. Conversely, a higher height (H) and larger slope (θ) resulted in greater energy consumption for airflow transport. Therefore, from the velocity gradient in Figure 10a–e, it can be inferred that H = 600 mm had the smallest velocity peak. The stacked bar chart in Figure 14 shows that the optimal range for suction chamber height was between 500 mm and 600 mm.

Table 3. Single-factor experimental results for suction chamber height.

H/mm	θ/°	v_j/m·s^{-1}	v_o/m·s^{-1}	v_m/m·s^{-1}	γ_v
450	56.31	7.649131	33.75902	16.8003	0.620519
500	59.09	8.235612	34.09176	18.25027	0.637646
550	61.35	8.751184	34.10965	17.52553	0.674940
600	63.43	8.465665	33.28181	17.50163	0.640138
650	65.26	8.106235	32.11111	16.71404	0.627712

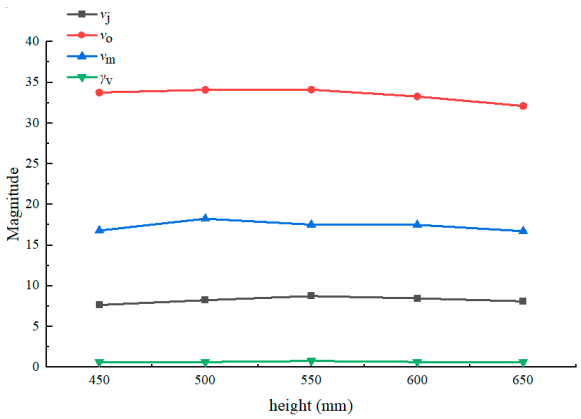

Figure 13. Results of various height indicators for the suction chamber.

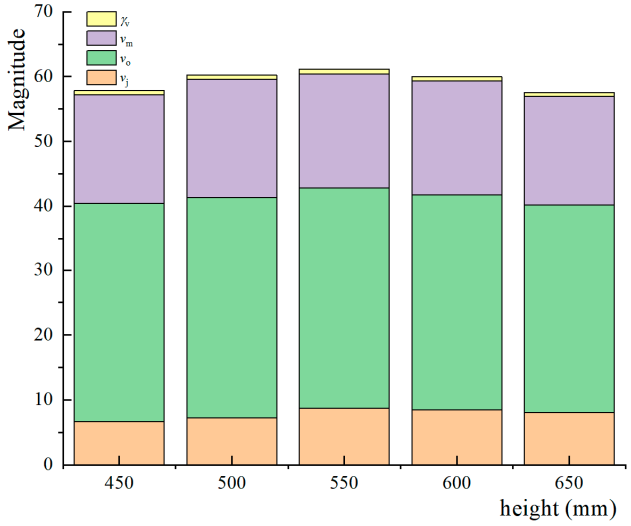

Figure 14. Stacked bar chart of various height indicators for the suction chamber.

3.3. Results and Analysis of Orthogonal Rotation Experiments

A variance analysis of the orthogonal experimental results is presented in Table 4. The results indicate that the regression models for v_j, v_o, and v_m are highly significant ($p < 0.01$), while the regression model for γ_v is not significant. This suggests that changes in the main factors have little impact on the uniformity of airflow in the suction chamber, so this factor was excluded from further consideration. The diameter of the straw outlet and the negative pressure at the outlet had a highly significant impact on the three indicators v_j, v_o, and v_m. The vertical height of the suction chamber also had a significant impact on these three test indicators. The order of importance of the various main factors on these three indicators was v_j, v_o, and v_m. After removing the non-significant terms, the regression equations for each factor concerning the indicators were as follows:

$$v_j = -0.206371 + 0.029020x_1 - 0.000727x_2 + 0.001393x_3 \tag{10}$$

$$\begin{aligned} v_o = \quad & -1915.49652 + 15.30079x_1 + 1.41175x_2 + 0.054322x \\ & -0.001031x_2^2 - 8.46191 \times 10^{-6}x_3^2 \end{aligned} \tag{11}$$

$$\begin{aligned} v_m = \quad & 134.73688 - 3.95186x_1 + 0.883007x_2 + 0.012654x_3 \\ & -0.002729x_1x_2 - 2.5 \times 10^{-5}x_2x_3 + 0.013649x_1^2 - 0.000252x_2^2 \\ & -1.25940 \times 10^{-6}x_3^2 \end{aligned} \tag{12}$$

A lack-of-fit test was performed on the above regression equations to demonstrate that there was no significant quadratic relationship ($p > 0.05$) between other factors and the test indicators.

As shown in Equation (10), the software recommended a multivariate linear regression equation for near-ground airflow velocity (v_j). This equation intuitively showed that within the range of experimental data, the near-ground airflow velocity was directly proportional to the straw outlet diameter and the negative pressure at the outlet, while it was inversely proportional to the vertical height of the suction chamber. This is because a greater negative pressure leads to greater suction, which aids ground-level airflow, and a higher suction chamber height increases the distance traveled from the top of the suction chamber to the ground, resulting in more energy loss and pressure drop.

Table 4. Variance analysis results for simulation experiments.

Test Index	Source	Sum of Squares	df	Mean Square	F-Value	*p*-Value
v_j	Model	4.06	3	1.35	62.16	<0.0001
	X_1	0.1684	1	0.1684	7.74	0.0179
	X_2	0.0106	1	0.0106	0.4856	0.5004
	X_3	3.88	1	3.88	178.25	<0.0001
	Residual	0.2394	11	0.0218		
	Lack of Fit	0.1874	9	0.0208	0.8007	0.6679
v_o	Model	87.05	9	9.67	7.70	0.0184
	X_1	1.42	1	1.42	1.13	0.3362
	X_2	4.30	1	4.30	3.42	0.1234
	X_3	41.22	1	41.22	32.82	0.0023
	X_2^2	24.54	1	24.54	19.54	0.0069
	X_3^2	16.52	1	16.52	13.15	0.0151
	Residual	6.28	5	1.26		
	Lack of Fit	6.05	3	2.02	17.84	0.0536
v_m	Model	18.96	9	2.11	128.11	<0.0001
	X_1	0.3846	1	0.3846	23.38	0.0047
	X_2	0.0773	1	0.0773	4.70	0.0824
	X_2	12.61	1	12.61	766.90	<0.0001
	X_1 X_2	1.86	1	1.86	113.18	0.0001
	X_2 X_3	1.59	1	1.59	96.63	0.0002
	X_1^2	0.4299	1	0.4299	26.14	0.0037
	X_2^2	1.47	1	1.47	89.12	0.0002
	X_3^2	0.3660	1	0.3660	22.25	0.0053
	Residual	0.0822	5	0.0164		
	Lack of Fit	0.0766	3	0.0255	9.10	0.1006
γ_v	Model	0.0214	9	0.0024	1.24	0.4274

Further analysis of v_o and v_m related experimental data was conducted to obtain significant interaction response surfaces, as shown in Figure 15, and to analyze them. As illustrated in Figure 15a,d, when the negative pressure was −3500 Pa, the maximum values of v_o and v_m occurred between H values of 500 and 550 mm, which aligns with the results from the single-factor optimization experiments in Section 2.4.3. As shown in Figure 15b,c, when the straw outlet diameter was 195 mm, both the straw outlet airflow velocity and YZ longitudinal section airflow velocity were positively correlated with the outlet negative pressure. This indicates that v_j, v_o, and v_m are all positively related to the outlet negative pressure, meaning that higher negative pressure is more advantageous for straw transportation. As depicted in Figure 15d, when the negative pressure was −3500 Pa, v_m was positively correlated with the straw outlet diameter. The reason for this might be that with a larger straw outlet diameter, there was a greater angle between the straw outlet horizontal plane and the chamber surface, which buffered the collision of the airflow with the chamber surface and helped reduce airflow pressure loss.

The experimental indicators were optimized using Design-Expert 12.0.1.0 software to obtain the best combination of suction chamber parameters. It was found that to achieve the best indicators, the negative pressure at the straw outlet should be maximized. However, it may not always be possible to reach the simulated fan total pressure value of −3500 Pa during actual operation. To measure the static pressure at the outlet of the air duct with diameters of 190 mm and 200 mm at maximum speed of 2900 r/min, a model JY3000 air velocity and air pressure tester was used. The results showed that the average static pressure ranged from −2750 Pa to −2900 Pa.

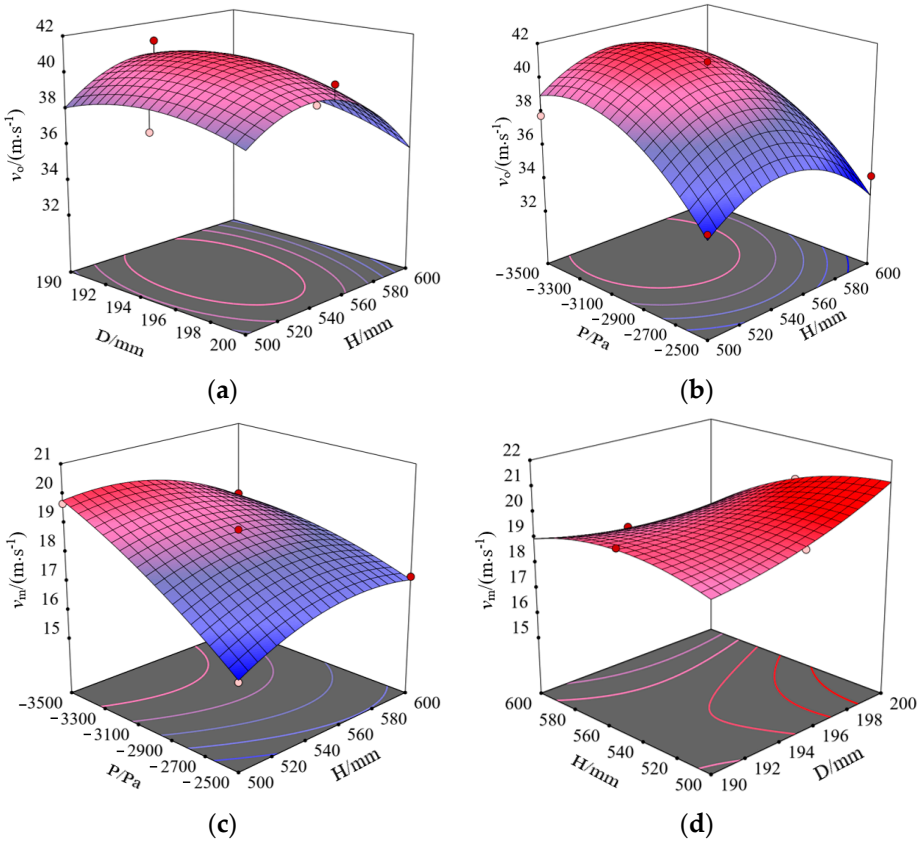

Figure 15. Bifactorial response surface. (**a**) $v_o = f(x_1, x_2, 500)$; (**b**) $v_o = f(195, x_2, x_3)$; (**c**) $v_m = f(195, x_2, x_3)$; (**d**) $v_m = f(x_1, x_2, 3500)$.

Considering the actual operational requirements of the straw collection unit, the objective function and constraints were selected as follows:

$$\begin{cases} \max v_j(x_1, x_2, x_3) \\ \max v_o(x_1, x_2, x_3) \\ \max v_m(x_1, x_2, x_3) \\ \max \gamma_v(x_1, x_2, x_3) \\ 190 \text{ mm} \le x_1 \le 200 \text{ mm} \\ 500 \text{ mm} \le x_2 \le 600 \text{ mm} \\ -2900 \text{ Pa} \le x_3 \le -2500 \text{ Pa} \end{cases} \tag{13}$$

The optimal parameter combination was obtained as follows: straw outlet diameter of 200 mm, suction chamber vertical height of 536.02 mm, and straw outlet negative pressure of −2900 Pa. The optimized values for the indicators were v_j = 9.25 m/s, v_o = 38.80 m/s, v_m = 19.14 m/s, and γ_v = 0.66.

To validate the reliability of the optimization results, simulations and bench validation experiments were conducted using the optimal parameter combination. In the experiments, the following parameters were set: the straw outlet diameter was 200 mm, the vertical height of the suction chamber was rounded to 536 mm for ease of manufacturing, the bottom diameter was 800 mm, resulting in a slope angle (θ) of 60.77°, and the straw outlet negative pressure was set at −2900 Pa.

The simulation test results were as follows: v_j = 9.238 m/s, v_o = 35.71 m/s, v_m = 17.79 m/s, γ_v = 0.61, and as shown in Figure 16, the lowest velocity in the middle region of near-ground airflow was approximately 12 m/s, which met the suspension velocity requirement for straw. Therefore, there was no problem with the straw initiation at the bottom of the optimized suction chamber. As shown in Figure 17, the minimum

negative pressure at the bottom of the optimized suction chamber in the green area was approximately −1500 Pa, which was significantly improved compared to the −1360 Pa in Figure 8. As shown in Figure 18, the maximum airflow velocity after optimization was approximately 57.6 m/s, which was greater than the maximum value obtained in the single-factor test shown in Figure 10.

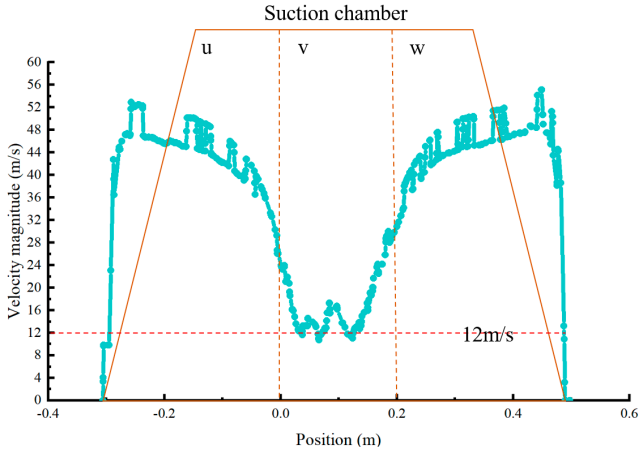

Figure 16. Curve chart of near-ground airflow velocity at suction chamber inlet after optimization.

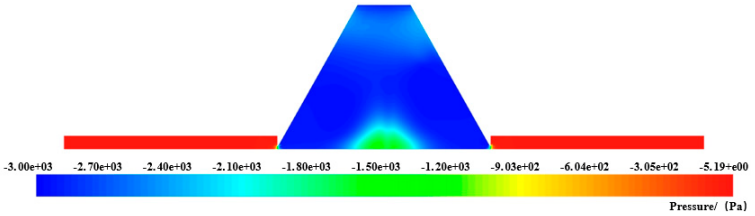

Figure 17. Static pressure contour plot on YZ vertical section after optimization.

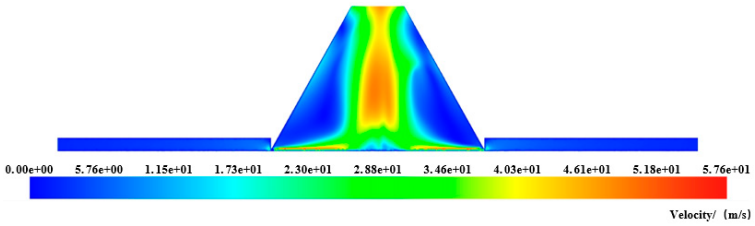

Figure 18. Velocity contour plot on YZ vertical section of the suction chamber after optimization.

3.4. Results of the Straw Suction Unit Test on the Bench Test

The inverter was used to adjust the fan speed to the maximum value of 2900 r/min. In the bench test of the apparatus shown in Figure 8, the results obtained from the wind speed, air volume, and air pressure measurements with the testing instrument were as follows: v_j = 9.03 m/s and v_o = 34.27 m/s, with an error of less than 5% compared to the simulation data.

For the average longitudinal section airflow velocity, difficulties in accurate measurement were encountered during the actual experiment, resulting in lower accuracy. However, based on the small error between the measured v_j and v_o and the simulation data, and considering the experiment's use of approximately 1.3 kg of straw spread on flat ground, the results indicated that these straw samples could be successfully suctioned into the collection bag, demonstrating that the optimization results met the basic requirements of the suction unit. The suction cavity is a complex three-dimensional structure, which causes non-uniformity in the air flow and flow velocity gradient. As a result, it is difficult

to find a suitable measurement point in the cavity to obtain a representative average velocity value v_m. Although there are advanced measurement technologies, such as laser Doppler velocimetry (LDV) and particle image velocimetry (PIV), which can measure airflow in three dimensions, they require expensive equipment and expertise [53–57]. In summary, accurate measurement of v_m and γ_v becomes complex and challenging due to the interaction of factors, such as the complexity of the flow structure in the suction cavity, non-uniformity, velocity gradient, measurement point selection, and complexity of the measurement technology. Therefore, it was not possible to accurately measure v_m and γ_v in this bench test. Verification of these parameters will occur in subsequent simulations and field tests. Comprehensive straw suction efficiency will be used as the benchmark for validation.

4. Conclusions

This study presented the design of a machine that detects the weight of straw cover. The operational process of the device was explained in detail. The study focused on the core component, the straw suction unit, and described its structure and working principles. An analysis of the movement and forces acting on straw within the suction chamber was conducted, identifying the factors that influence the efficiency of straw suction. These factors include suction chamber structural parameters and transport pressure.

In order to design the straw suction unit, the key components were considered based on the straw stem suspension velocity range of 5.081 m/s to 11.813 m/s. This allowed for calculations of the wind duct diameter, suction chamber structure, and fan selection. The wind duct diameter was approximated as 0.2 m. As a result, the 06-46 3.6A model centrifugal fan was chosen for the experiments.

A model of a suction chamber was constructed and several pre-experiments were conducted. CFD single-factor optimization simulations and orthogonal rotation combination tests were used to determine the optimal parameter combination for achieving the best straw transport effect. The results of the study showed that the ideal parameter combination consisted of an outlet diameter of 200 mm, an outlet negative pressure of −2900 Pa, and a suction chamber vertical height of 536.02 mm. Under these conditions, the velocity of the near-ground airflow v_{j} was 9.25 m/s, the outlet velocity v_{o} was 38.80 m/s, and the longitudinal section airflow velocity v_{m} was 19.14 m/s, with a velocity uniformity index γ_{v} of 0.66.

Based on simulation tests and bench verification tests, it was found that when setting the fan to a maximum working speed of 2900 r/min, the optimal suction unit parameters were an outlet diameter of 200 mm, a suction chamber vertical height of 536 mm, a base diameter of 800 mm, and a slope of 60.77°. This optimization resulted in v_{j} = 9.03 m/s and v_{o} = 34.27 m/s, which met the basic requirements for the straw suction unit.

These findings provide fundamental parameters and references for the further optimization of the straw cover weight detection machine's straw suction unit. This study only analyzed the straw suction unit theoretically and experimentally on a single object of straw. However, it did not take into account factors such as soil and impurities. In order to improve the accuracy of the straw coverage detection machine, further research should be conducted on how to reduce the suction rate of soil and impurities while ensuring the straw suction rate.

Author Contributions: Conceptualization, R.L.; writing—original draft preparation, R.L. and H.L.; writing—review and editing, C.L., C.W., Z.W., Z.T., D.L. and S.J. All authors have read and agreed to the published version of this manuscript.

Funding: This research was funded by the China Agriculture Research System of MOF and MARA (Grant No. CARS-03) and the 2115 Talent Development Program of China Agricultural University and Chinese Universities Scientific Fund (Grant No. 2021TC105).

Institutional Review Board Statement: Not applicable.

Data Availability Statement: Not applicable.

Acknowledgments: We would like to express our gratitude to all the members of the Conservation Tillage Research Centre. Additionally, we sincerely appreciate the work of the editor and the reviewers of this paper.

Conflicts of Interest: The authors declare no conflict of interest.

References

1. Kassam, A.; Friedrich, T.; Shaxson, F.; Pretty, J. The spread of Conservation Agriculture: Justification, sustainability, and uptake. *Int. J. Agric. Sustain.* **2009**, *7*, 292–320. [CrossRef]
2. He, J.; Li, H.; Chen, H.; Lu, C.; Wang, Q. Research progress of conservation tillage technology and machine. *Trans. Chin. Soc. Agric. Mach.* **2018**, *49*, 1–19.
3. Zong, J. *Conservation Tillage in China*; China Agricultural Press: Beijing, China, 2008; pp. 3–4; ISBN 978-7-109-12815-6.
4. Ranaivoson, L.; Naudin, K.; Ripoche, A.; Affholder, F.; Rabeharisoa, L.; Corbeels, M. Agro-ecological functions of crop residues under conservation agriculture A review. *Agron. Sustain. Dev.* **2017**, *37*, 26. [CrossRef]
5. Indoria, A.K.; Rao, C.S.; Sharma, K.L.; Reddy, K.S. Conservation agriculture—A panacea to improve soil physical health. *Curr. Sci.* **2017**, *112*, 52–61. [CrossRef]
6. Karlen, D.L.; Wollenhaupt, N.C.; Erbach, D.C.; Berry, E.C.; Swan, J.B.; Eash, N.S.; Jordahl, J.L. Crop residue effects on soil quality following 10-years of no-till corn. *Soil Tillage Res.* **1994**, *31*, 149–167. [CrossRef]
7. Mbah, C.N.; Nneji, R.K. Effect of different crop residue management techniques on selected soil properties and grain production of maize. *Afr. J. Agric. Res.* **2011**, *6*, 4149–4152.
8. Liu, X.; Liu, H.; Wang, Q. Method and test of straw coverage detection in farmland. *J. Chin. Agric. Mach.* **2021**, *42*, 203–208.
9. Li, J.; LÜ, C.; Yuan, Y. Fast Fourier transform combined with SVM algorithm to identify surface maize straw coverage. *Trans. CSAE* **2019**, *35*, 194–201.
10. Cai, W.; Zhao, S.; Wang, Y. Estimation of winter wheat residue coverage using optical and SAR remote sensing images. *Remote Sens.* **2019**, *11*, 1163. [CrossRef]
11. Gao, L.; Zhang, C.; Yun, W. Mapping crop residue cover using adjust normalized difference residue index based on Sentinel-2 MSI dat. *Soil Tillage Res.* **2022**, *220*, 105374. [CrossRef]
12. Shi, Y.; Luo, W.; Hu, Z. Design and test of equipment for straw crushing with strip-laying and seed-belt classification with cleaning under full straw mulchin. *Trans. Chin. Soc. Agric. Mach.* **2019**, *50*, 58–67.
13. Wang, J.; Gao, Y.; Yang, S. Algorithm of for 2D maximum between-cluster image segmentation based on GA. *Microcomput. Appl.* **2011**, *32*, 24–30.
14. Zhu, Q.; Xu, X.; Sun, Z. Estimation of winter wheat residue coverage based on GF-1 imagery and machine learning algorithm. *Agronomy* **2022**, *12*, 1051. [CrossRef]
15. An, X.; Wang, P.; Luo, C. Corn straw coverage calculation algorithm based on k-means clustering and zoning optimization method. *Trans. Chin. Soc. Agric. Mach.* **2021**, *52*, 84–89.
16. Shi, N.; Chen, H.; Wei, Z. Design and experiment of stalk returning proportion adjusting device for corn original stubble. *Trans. Chin. Soc. Agric. Eng.* **2020**, *36*, 11–22.
17. Cai, L.; Zhang, J.; Gai, Z. Effect of the amount of stalk return to field on soil enzyme activities under no-tillage. *Chin. J. Soil Sci.* **2015**, *46*, 1127–1132.
18. Wang, Q.; Wang, X.; Li, H. Effect of maize straw mulching on winter wheat growth in double cropping area of northern China. *Trans. Chin. Soc. Agric. Mach.* **2017**, *48*, 192–198.
19. Zhou, D.; Li, M.; Li, Y.; Qi, J.; Liu, K.; Cong, X.; Tian, X. Detection of ground straw coverage under conservation tillage based on deep learning. *Comput. Electron. Agric.* **2020**, *172*, 105369. [CrossRef]
20. Morrison, J.E.; Huang, C.H.; Lightle, D.T.; Daughtry, C. Residue Measurement Techniques. *J. Soil Water Conserv.* **1993**, *48*, 478–483.
21. Laamrani, A.; Lara, R.P.; Berg, A.A.; Branson, D.; Joosse, P. Using a mobile device "app" and proximal remote sensing technologies to assess soil cover fractions on agricultural fields. *Sensors* **2018**, *18*, 708. [CrossRef]
22. Liu, Y.; Zhang, S.; Yu, H.; Wang, Y.; Wang, J. Straw detection algorithm based on semantic segmentation in complex farm scenarios. *Opt. Precis. Eng.* **2020**, *28*, 200–211.
23. Su, Y.; Zhang, D.; Li, H.; He, J.; Wang, Q.; Li, H. Straw cover rate detection system based on automatic threshold segmentation algorithm. *J. Agric. Mech. Res.* **2012**, *34*, 138–142.
24. Liu, Y.; Sun, J.; Zhang, S.; Yu, H.; Wang, Y. Detection of straw coverage based on multi-threshold and multi-target UAV image segmentation optimization algorithm. *Trans. Chin. Soc. Agric. Eng.* **2020**, *36*, 134–143.
25. Li, H.; Li, R. A Self-Propelled Straw Cover Weight Machine and Detection Method. Chinese Patent CN 116295761 A, 23 June 2023.
26. Tang, Z.; Zhang, B.; Liu, X.; Ren, H.; Li, X.Y.; Li, Y.M. Structural model and bundling capacity of crawler picking and baling machine for straw wasted in field. *Comput. Electron. Agric.* **2020**, *175*, 105622. [CrossRef]
27. Zheng, Z.; He, J.; Wang, Q.; Li, H.; Li, W.; Chen, W. Design and experiment on straw pick-chopping and ditch-burying integrated machine. *Chin. Soc. Agric. Mach.* **2017**, *48*, 87–96.

28. Yang, Q.; Chen, G.; Xie, L.; Wang, Q.; He, J.; Li, H. Design and experiment of telescopic finger stalk of maize straw burying machine. *Chin. Soc. Agric. Mach.* **2020**, *51*, 35–43.
29. Tian, Y.; Lin, J.; Li, B. Design and test of conveying device of pneumatic straw deep burying and returning machine. *Chin. Soc. Agric. Mach.* **2018**, *49*, 36–44.
30. Su, J.; Zhou, C.J.; Jiang, X.H.; Qiao, Z.Z. Orderly arrangement of agricultural biomass particles in designed gas-solid fluidized beds using CFD-DEM and image experiment. *Comput. Electron. Agric.* **2023**, *204*, 107510. [CrossRef]
31. Aarseth, K.A. Attrition of feed pellets during pneumatic conveying: The influence of velocity and bend radius. *Biosyst. Eng.* **2004**, *89*, 197–213. [CrossRef]
32. Gomes, T.; Lourenco, G.A.; Ataide, C.H.; Duarte, C.R. Biomass feeding in a dilute pneumatic conveying system. *Powder Technol.* **2021**, *391*, 321–333. [CrossRef]
33. Guner, M. Pneumatic conveying characteristics of some agricultural seeds. *J. Food Eng.* **2007**, *80*, 904–913. [CrossRef]
34. Raheman, H.; Jindal, V.K. Pressure drop gradient and solid friction factor in horizontal pneumatic conveying of agricultural grains. *Appl. Eng. Agric.* **2001**, *17*, 649–656. [CrossRef]
35. Malekjani, N.; Jafari, S.M. Simulation of food drying processes by Computational Fluid Dynamics (CFD); recent advances and approaches. *Trends Food Sci. Technol.* **2018**, *78*, 206–223. [CrossRef]
36. Duarte, C.; de Souza, F.J. Innovative pipe wall design to mitigate elbow erosion: A CFD analysis. *Wear* **2017**, *380–381*, 176–190. [CrossRef]
37. Bournet, P.E.; Rojano, F. Advances of Computational Fluid Dynamics (CFD) applications in agricultural building modelling: Research, applications and challenges. *Comput. Electron. Agric.* **2022**, *201*, 107277. [CrossRef]
38. Zhu, Y. *Metallurgical Equipment*; Metallurgical Industry Press: Beijing, China, 2009; pp. 9–11; ISBN 978-7-5024-4933-9.
39. Chen, W.; Zhang, W. *Fluid Mechanics*; Tianjin University Press: Tianjin, China, 2004; pp. 164–165; ISBN 7-5618-1895-5.
40. Zhou, N.; Zhu, F. *Principles and Design Calculations of Pneumatic Conveying*; Henan Science and Technology Press: Zhengzhou, China, 1981; pp. 123–124.
41. Beijing Iron and Steel Institute. *Pneumatic Conveying Device*; People's Communications Press: Beijing, China, 1974; pp. 100–101.
42. Prandtl, L. *Introduction to Fluid Mechanics*; Science Press: Beijing, China, 2016; pp. 187–194; ISBN 978-7-03-046976-2.
43. Tao, J. *Engineering Fluid Mechanics: Pumps and Fans*; Beijing Institute of Technology Press: Beijing, China, 2021; pp. 99–103; ISBN 978-7-5763-0233-2.
44. Reichardt, H. The heat transfer in turbulent friction layers. *Z. Fur Angew. Math. Und Mech.* **1940**, *20*, 297–328. [CrossRef]
45. Yang, Z. Research on Pneumatic Separation and Rheological Characteristic under Compression Molding of Corn Straw'main Components. Ph.D. Thesis, Northwest A&F University, Xianyang, China, 2011.
46. Zhou, Z. *Agricultural Materials Science*; Agriculture Press: Beijing, China, 1994; pp. 88–93; ISBN 7-109-02717-1.
47. Jin, H.; Li, J. Study of impurity removal from corn mixture. *Chem. World* **2012**, *53*, 214–218.
48. Hou, H.; Cui, Q.; Guo, Y.; Zhang, Y.; Sun, D.; Lai, S.; Liu, J. Design and test of air-sweeping suspension velocity testing device for cleaning threshed materials of grain and oil crops. *Trans. Chin. Soc. Agric. Eng.* **2018**, *34*, 43–49.
49. Zhao, X.; Chen, Y.; Zhang, S. *Agro-Materials Science*; Machinery Industry Press: Beijing, China, 1987; pp. 78–84; ISBN 15033·7126.
50. Huang, B. *Pneumatic Conveying*; Shanghai Scientific & Technical Publishers: Shanghai, China, 1984; pp. 84–112; ISBN 15119·2296.
51. ХОДЕЕВ, Н.Е. Calculation method for pressure loss of accelerated materials during pneumatic conveying. *Oil Technol.* **1979**, *1*, 103–104.
52. Li, T.; Jin, S.; Huang, S.; Liu, W. Evaluation indices of flow velocity distribution uniformity: Comparison and application. *Therm. Power Gener.* **2013**, *42*, 60–63.
53. Cao, X.; Liu, J.; Jiang, N.; Chen, Q. Particle image velocimetry measurement of indoor airflow field: A review of the technologies and applications. *Energy Build.* **2014**, *69*, 367–380. [CrossRef]
54. Cao, G.; Sivukari, M.; Kurnitski, J.; Ruponen, M.; Seppänen, O. Particle Image Velocimetry (PIV) application in the measurement of indoor air distribution by an active chilled beam. *Build. Environ.* **2010**, *45*, 1932–1940. [CrossRef]
55. Giancola, E.; Sánchez, M.; Friedrich, M. Possibilities and challenges of different experimental techniques for airflow characterisation in the air cavities of façades. *J. Facade Des. Eng.* **2018**, *6*, 34–48.
56. Li, Z.; Chang, W.; Gao, C.; Hao, Y. A novel five-wire micro anemometer with 3D directionality for low speed air flow detection and acoustic particle velocity detecting capability. *J. Micromech. Microeng* **2018**, *28*, 044004. [CrossRef]
57. Fu, S.; Biwole, P.; Mathis, C. Particle tracking velocimetry for indoor airflow field: A review. *Build. Environ.* **2015**, *87*, 34–44. [CrossRef]